Advanced Composite Materials
Publication details, including instructions for authors and subscription information:
http://www.tandfonline.com/loi/tacm20

A Simple Approach for Determining the Characteristic Distance in the Point Stress Criterion for Holed CFRP Unidirectional Laminates

S. Yashiro [a], K. Ogi [b], T. Yamamoto [c] & T. Watanabe [d]

[a] Graduate School of Science and Engineering, Ehime University, 3 Bunkyo-cho, Matsuyama, Ehime 790-8577, Japan

[b] Graduate School of Science and Engineering, Ehime University, 3 Bunkyo-cho, Matsuyama, Ehime 790-8577, Japan

[c] Faculty of Engineering, Fukuoka University, 8-19-1 Nanakuma, Jonan-ku, Fukuoka 814-0180, Japan

[d] Graduate School of Science and Engineering, Ehime University, 3 Bunkyo-cho, Matsuyama, Ehime 790-8577, Japan

Version of record first published: 02 Apr 2012.

To cite this article: S. Yashiro , K. Ogi , T. Yamamoto & T. Watanabe (2010): A Simple Approach for Determining the Characteristic Distance in the Point Stress Criterion for Holed CFRP Unidirectional Laminates, Advanced Composite Materials, 19:3, 243-259

To link to this article: http://dx.doi.org/10.1163/092430409X12605406698318

VSP

Advanced Composite Materials 19 (2010) 243–259

ADVANCED COMPOSITE MATERIALS
brill.nl/acm

A Simple Approach for Determining the Characteristic Distance in the Point Stress Criterion for Holed CFRP Unidirectional Laminates

S. Yashiro [a,*], **K. Ogi** [a], **T. Yamamoto** [b] **and T. Watanabe** [a]

[a] Graduate School of Science and Engineering, Ehime University, 3 Bunkyo-cho, Matsuyama, Ehime 790-8577, Japan

[b] Faculty of Engineering, Fukuoka University, 8-19-1 Nanakuma, Jonan-ku, Fukuoka 814-0180, Japan

Received 20 April 2009; accepted 14 July 2009

Abstract

This paper presents a fracture criterion for predicting the strength of a CFRP unidirectional laminate with a hole. We formulated the point stress criterion (PSC) for notched composites with the characteristic distance at which the Tsai–Hill criterion for orthotropic materials was satisfied. The strengths of CFRP off-axis unidirectional laminates with a hole predicted by the PSC agreed well with the measured strengths, and the validity of the characteristic distance determined by the Tsai–Hill criterion was confirmed. Moreover, we observed the fractured surfaces of the holed specimens with small off-axis angles and found that the fracture mode within the characteristic distance (fiber breakage mode) was different from that away from the hole (shear fracture mode). These observations of the fractured surfaces suggested that the characteristic distance represented the size of the initially damaged area at the notch tip.

Keywords

Polymer–matrix composites (PMCs), strength, failure criterion, stress concentrations, fractography

1. Introduction

Carbon fiber reinforced plastics (CFRPs) have frequently been applied to various structures and have replaced conventional metals as structural materials, taking advantage of their light weight, high strength and modulus, and superior fatigue properties. The internal microstructure of a material and the microscopic damage extension cannot be neglected when the intrinsic strength of a composite material is discussed. However, in a structural design, it is not always possible to perform

* To whom correspondence should be addressed. E-mail: yashiro.shigeki@eng.ehime-u.ac.jp
Edited by the JSCM

 DOI:10.1163/092430409X12605406698318

a structural analysis with damage extension. A simple estimation of the strength by a fracture criterion is often useful in a practical design flow rather than a detailed fracture simulation.

A notch can exist in a structural component by necessity. Predictions and experiments of notched composite laminates were reviewed in detail by Awerbuch and Madhukar [1]. Among various fracture criteria, the average stress criterion (ASC) and the point stress criterion (PSC) [2–4] have widely been used. In these criteria, it is assumed that failure occurs when the average stress within a given distance from the notch tip or the stress at a given distance (characteristic distance) exceeds the strength of the unnotched laminate. Huh and Hwang [5] predicted the fatigue life of circular notched quasi-isotropic CFRP laminates based on the PSC (ASC) with a residual strength degradation model and assumption of the stress-redistribution. Belmonte *et al.* [6, 7] investigated the notched strength of woven quasi-isotropic laminates, and indicated that the characteristic distance of the ASC was similar to the critical damage zone length given by a physically-based damage growth model. On the other hand, the Tsai–Hill criterion [8] and the Tsai–Wu criterion [9] are well known as fracture criteria for orthotropic materials; the off-axis strength of unidirectional laminates has been predicted by these criteria. However, few fracture criteria have been proposed that predict the off-axis strength of notched unidirectional laminates, and the notched strength was underestimated by the Tsai–Hill criterion or the Tsai–Wu criterion [10]. Tanaka *et al.* [10, 11] proposed an extended average stress criterion that predicted the off-axis strength of a notched CFRP unidirectional laminates.

Ogi *et al.* [12] investigated the relation between the PSC and the Tsai–Hill criterion to predict the notched strength of a unidirectional discontinuous fiber reinforced plastics, and demonstrated that the PCS with the characteristic distance determined by the Tsai–Hill criterion was valid for the strength estimation. They also indicated that the PSC with well-defined characteristic distance was equivalent to the criterion by the linear notch mechanics [13–15]. These discussions should be confirmed for continuous fiber reinforced plastics, since CFRPs with continuous fibers, which have been applied to primary components in aircraft and other structures, have large orthotropic properties compared to the short-fiber composites used in the previous study [12]. In addition, the physical meaning of the characteristic distance in the fracture criterion has not been clarified in the previous studies.

Therefore, the purpose of the present study is to investigate the relation between the PSC and the Tsai–Hill criterion in off-axis CFRP laminates with a hole and then to clarify the physical meaning of the characteristic distance. First, we formulated the PSC that conformed to the Tsai–Hill criterion in Section 2. Next, the experimental and analysis procedures were described in Sections 3 and 4. In Section 5, we applied this fracture criterion to the tensile strength of the holed unidirectional laminates with some off-axis angles, and verified the characteristic distance determined in this study. Finally, the observations of fractured surfaces were presented to discuss the physical meaning of the characteristic distance.

2. Fracture Criterion

2.1. Tsai–Hill Criterion

This section introduces the equations for predicting the tensile strength of a notched unidirectional laminate derived from the Tsai–Hill criterion; the detailed derivation processes are presented in the Appendix. In the present study, a unidirectional specimen with a hole (radius ρ) is investigated, and the longitudinal direction is defined as the x-direction. The material principal coordinate (1–2) is rotated by angle θ from the global coordinate x–y as depicted in Fig. 1. The Tsai–Hill criterion for an orthotropic plate under the plane stress condition is expressed by using the strengths of the unidirectional lamina:

$$\left(\frac{\sigma_1}{\sigma_{1\mathrm{u}}}\right)^2 + \left(\frac{\sigma_2}{\sigma_{2\mathrm{u}}}\right)^2 - \frac{\sigma_1\sigma_2}{(\sigma_{1\mathrm{u}})^2} + \left(\frac{\sigma_6}{\sigma_{6\mathrm{u}}}\right)^2 = 1, \tag{1}$$

where $\sigma_{1\mathrm{u}}$ is the longitudinal strength, $\sigma_{2\mathrm{u}}$ is the transverse strength, and $\sigma_{6\mathrm{u}}$ is the in-plane shear strength. Although this criterion cannot distinguish the tension and the compression, we used the Tsai–Hill criterion for simplicity since only the tensile stress is applied in this study. The other improved criterion, such as the Tsai–Wu criterion, should be used if a complex loading case including compression was considered. We can obtain the nominal stress when the Tsai–Hill criterion is satisfied at point R (distance r from the notch tip) as follows:

$$\sigma_{\mathrm{n,TH}}(r, \rho, \theta) = \frac{1}{\sqrt{\left(\frac{K_{1\mathrm{r}}}{\sigma_{1\mathrm{u}}}\right)^2 + \left(\frac{K_{2\mathrm{r}}}{\sigma_{2\mathrm{u}}}\right)^2 - \frac{K_{1\mathrm{r}}K_{2\mathrm{r}}}{(\sigma_{1\mathrm{u}})^2} + \left(\frac{K_{6\mathrm{r}}}{\sigma_{6\mathrm{u}}}\right)^2}}. \tag{2}$$

Here, $K_{i\mathrm{r}}$ $(i = 1, 2, 6)$ is the ratio of the stress component in the principal axes to the nominal stress, or the stress concentration factor for each direction. In this case, the stress σ_x at point R is represented as

$$\sigma_{\mathrm{r,TH}}(r, \rho, \theta) = \frac{m^2K_{1\mathrm{r}} + n^2K_{2\mathrm{r}} - 2mnK_{6\mathrm{r}}}{\sqrt{\left(\frac{K_{1\mathrm{r}}}{\sigma_{1\mathrm{u}}}\right)^2 + \left(\frac{K_{2\mathrm{r}}}{\sigma_{2\mathrm{u}}}\right)^2 - \frac{K_{1\mathrm{r}}K_{2\mathrm{r}}}{(\sigma_{1\mathrm{u}})^2} + \left(\frac{K_{6\mathrm{r}}}{\sigma_{6\mathrm{u}}}\right)^2}}, \tag{3}$$

where $m = \cos\theta$ and $n = \sin\theta$.

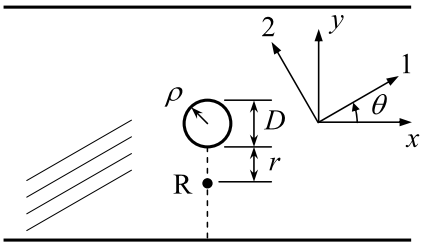

Figure 1. Coordinate systems in an off-axis specimen.

The off-axis strength of an unnotched specimen under the uniaxial tensile stress, σ_u, is represented as the tensile stress σ_x that satisfies the Tsai–Hill criterion, and we obtain:

$$\sigma_u(\theta) = \frac{1}{\sqrt{\frac{m^2(m^2-n^2)}{(\sigma_{1u})^2} + \frac{n^4}{(\sigma_{2u})^2} + \frac{m^2n^2}{(\sigma_{6u})^2}}}. \tag{4}$$

2.2. Point Stress Criterion (PSC)

The PSC with the characteristic distance r^* has been verified for various FRPs with continuous fibers [2–4]. This study combined the Tsai–Hill criterion with the PSC, and the notched specimen is assumed to break when the stress field at point R* (distance r^* from the notch tip) satisfies the Tsai–Hill criterion. The above fracture criterion can be written as

$$\sigma_r^* = K_r(r^*, \rho, \theta)\sigma_{n,TH}(r^*, \rho, \theta) = \sigma_{r,C}(r^*, \rho, \theta), \tag{5}$$

$$K_r(r, \rho, \theta) = m^2K_{1r} + n^2K_{2r} - 2mnK_{6r}, \tag{6}$$

where σ_r^* is the stress component σ_x at point R*; $\sigma_{r,C}$ is the critical value of σ_r^* and is obtained by setting $r = r^*$ in equation (3).

In this study, we employed the strength σ_{iu} ($i = 1, 2, 6$) measured in experiments, and the ratio of the stress component to the nominal stress $K_{ir}(r, \rho, \theta)$ calculated by the finite-element analysis. Furthermore, the characteristic distance r^* was determined by using the Tsai–Hill criterion as discussed in the following sections.

3. Experimental

The material used was carbon fiber reinforced epoxy composite (T700S/#2521R, Toray Industries; fiber volume fraction of 60%) with a stacking sequence of $[\theta_8]$, where θ was the off-axis angle. A flat plate of a unidirectional laminate was manufactured from prepreg sheets by hot-pressing process (120°C, 2 h) in a vacuum chamber. Some specimens with off-axis angles of $\theta = 0°, 15°, 30°, 45°, 60°$ and 90° were prepared for tensile tests. A specimen with an off-axis angle θ is termed a θ-specimen in this study.

Figure 2 depicts the dimensions of a coupon specimen for the tensile tests. Coupon specimens were cut out from the flat plate by a diamond saw and were holed at the center by a drill. The edges of a specimen were polished by sand papers. The specimens were 200 mm long and 20 mm wide with a hole diameter D (= 2, 4, 6 mm). GFRP tabs were glued to the end of the specimen; oblique tabs proposed by Sun *et al.* [16, 17] were used in order to reduce the shear-coupling effects. The oblique angle of the tab, ϕ, is determined by

$$\cot\phi = -\bar{S}_{16}/\bar{S}_{11} = -\eta_{xy}, \tag{7}$$

where $\bar{S}_{ij}$ are the components of the compliance matrix in the material's principal coordinate, and η_{xy} is the coefficient of shear coupling. The material properties listed in Table 1 were used to calculate the inclined angle of the tab.

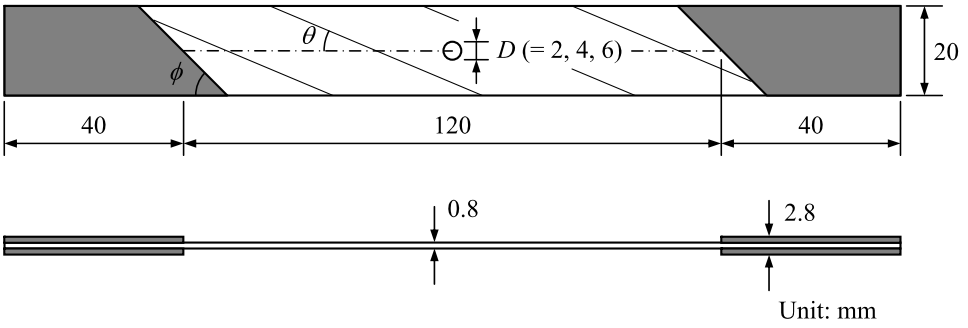

Figure 2. Geometry of a CFRP off-axis specimen with a hole.

Table 1.
Material properties of CFRP laminate

Longitudinal Young's modulus, E_1 (GPa)	135.0
Transverse Young's modulus, E_2 (GPa)	8.2
In-plane shear modulus, G_{12} (GPa)	4.8
In-plane Poisson's ratio, ν_{12}	0.31
Out-of-plane Poisson's ratio, ν_{23}	0.49

Quasi-static tensile tests were conducted for the CFRP unidirectional specimens at room temperature under the cross-head speed of 0.5 mm/min. The off-axis strength of unnotched specimens, σ_u, and the notched strength of holed specimens, $\sigma_{n,C}$, were experimentally measured for some off-axis angles. After the tensile tests, the fractured surfaces were observed by scanning electron microscopy (SEM).

4. Analysis

The stress distribution near the hole was analyzed by the finite-element analysis. Multipurpose finite-element analysis software (MSC.Marc 2001) was used in this study. Figure 3 depicts the finite-element model for the hole radius $D = 4$ mm. The entire specimen was modeled because of the non-symmetric stress distribution near the hole of an off-axis specimen. The dimensions were 200 mm in the longitudinal (x) direction and 20 mm in the transverse (y) direction. Four-node plane stress elements were used in this analysis; the detailed mesh pattern was applied to the region near the hole to precisely evaluate the stress concentration. The total numbers of nodal points were 42 476, 39 916, 37 356, and the total numbers of elements were 42 192, 39 632, 37 072 for the hole radius of 2, 4, 6 mm, respectively. Uniform tensile displacement was applied to the upper edge of the model, while the lower edge was fixed. Material properties listed in Table 1 were used in this analysis; linear elastic orthotropic behavior was assumed for all the elements.

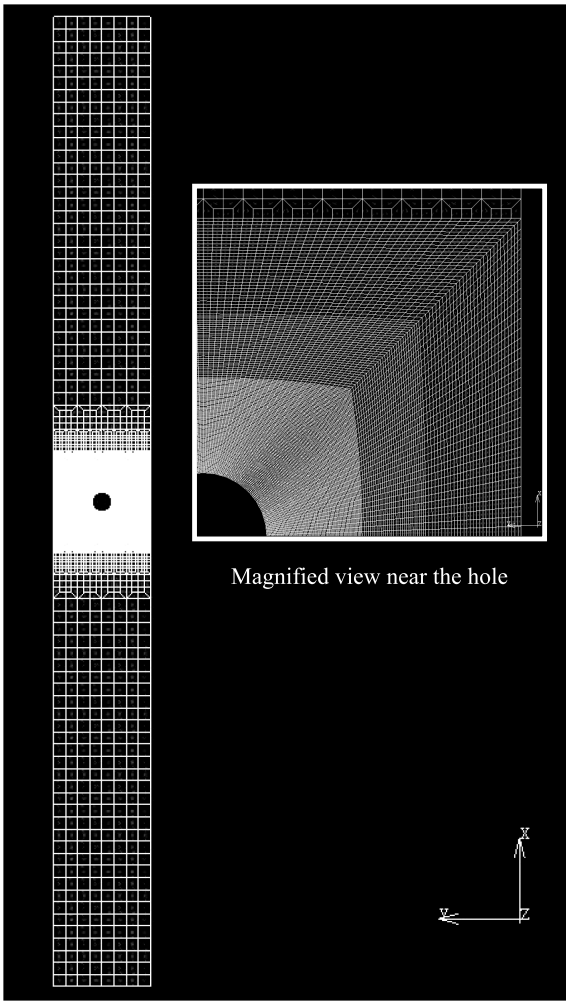

Figure 3. Finite-element model of the holed specimen.

The ratio of the stress in the principal coordinate to the nominal stress at the intact condition, $K_{i\mathrm{r}}$ $(i = 1, 2, 6)$, was calculated along the y-direction in the minimum cross-section, while the nominal stress was obtained from the sum of the nodal force at the loading edge. The stress concentration factor in the x-direction, K_{r}, and the nominal stress when the Tsai–Hill criterion was satisfied at point R (distance r from the hole edge) were then calculated from the analyzed $K_{i\mathrm{r}}$. Stress concentration factor at the hole edge, K_{t}, is needed to predict the strength by the PSC, and is written as

$$K_{\mathrm{t}}(\rho, \theta) = K_{\mathrm{r}}(0, \rho, \theta) = m^2 K_{1\mathrm{t}} + n^2 K_{2\mathrm{t}} - 2mn K_{6\mathrm{t}}, \tag{8}$$

where $K_{i\mathrm{t}}$ $(i = 1, 2, 6)$ is the stress concentration factor for each direction at the hole edge, i.e., $K_{i\mathrm{r}}(0, \rho, \theta)$.

The stress concentration factor at the hole edge is also obtained analytically for an orthotropic infinite plate [18] as

$$K_{\mathrm{t}}^{\infty} = 1 + \sqrt{2\left(\sqrt{\frac{E_x}{E_y}} - \nu_{xy}\right) + \frac{E_x}{G_{xy}}}. \tag{9}$$

Here, E_x (E_y) is the Young's modulus along the x (y) direction, ν_{xy} is the Poisson's ratio, and G_{xy} is the shear modulus.

5. Results and Discussion

5.1. Experimental Results

Figure 4 depicts the tensile strength for the unnotched specimens, σ_{u}, with some off-axis angles. The average strengths were $\sigma_{1\mathrm{u}} = 2736.7$ MPa for the 0°-specimen and $\sigma_{2\mathrm{u}} = 56.6$ MPa for the 90°-specimen. The shear strength was then estimated as $\sigma_{6\mathrm{u}} = 54.2$ MPa by fitting equation (4) to the strengths for all the off-axis angles. Figure 5 depicts the strength of the holed specimens, where the stress was evaluated by the minimum cross-sectional area. Notched strength $\sigma_{\mathrm{n,C}}$ had little dependency on the hole diameter D. The average strength ratio $\beta = \sigma_{\mathrm{n,C}}/\sigma_{\mathrm{u}}$ is then plotted in Fig. 6, where σ_{u} fitted by equation (4) is used. The strength ratio β decreased with increasing off-axis angle unlike the discontinuous GFRP [12]. However, β also had little dependency on the hole diameter D; this tendency was similar to the results of discontinuous GFRP.

Figure 7 depicts the typical fracture patterns of unnotched specimens and holed specimens ($D = 4$ mm). The 0°-specimens broke with progressive fiber breakages and splitting. The fracture behavior of the holed 0°-specimens was similar to that of the unnotched specimen, and fiber breakages and multiple splits were observed. A crack was generated and simultaneously extended along the fiber direction in the unnotched off-axis specimens and 90°-specimens. This fracture behavior was also

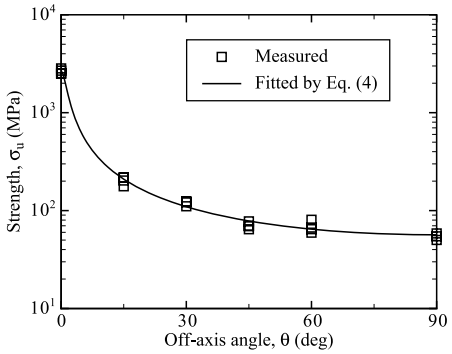

Figure 4. Measured tensile strength of intact specimens as a function of the off-axis angle θ. The experiment results were fitted by the Tsai–Hill criterion with $\sigma_{6\mathrm{u}} = 54.2$ MPa.

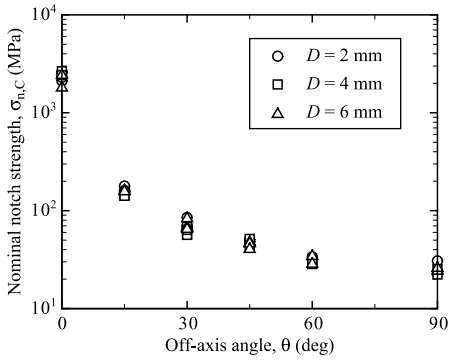

Figure 5. Measured tensile strength of holed specimens as a function of the off-axis angle θ.

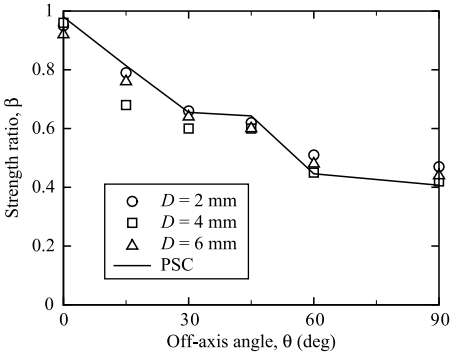

Figure 6. The ratio β of the strength for a holed off-axis specimen to the intact specimen. The measured strength ratio was compared with the prediction by the PSC.

observed in the holed off-axis specimens, and the crack was generated at the hole edge. The same fracture patterns were observed in the specimens with the other hole diameters.

5.2. Analysis Results

Figure 8 illustrates the distribution of the stress concentration factor in the x-direction, K_r, in the minimum cross-section for the hole diameter $D = 2$ mm. The larger stress concentration factor was calculated in the smaller off-axis angle. However, the effects of the off-axis angle on the stress concentration rapidly decreased as the distance r increased, and little dependency on θ was observed at the point $r > 2\rho$. Similar results were obtained in the other hole diameters.

The stress concentration factor at the hole edge, K_t, is illustrated in Fig. 9. Equation (9) indicated that this factor ($K_t = K_t^\infty$) was independent of the hole diameter D. However, the larger K_t was calculated for the larger hole diameter D, since the finite width was considered in the analysis. Although the definition of the nominal stress in this study suggested $K_t < K_t^\infty$, the results were opposite at

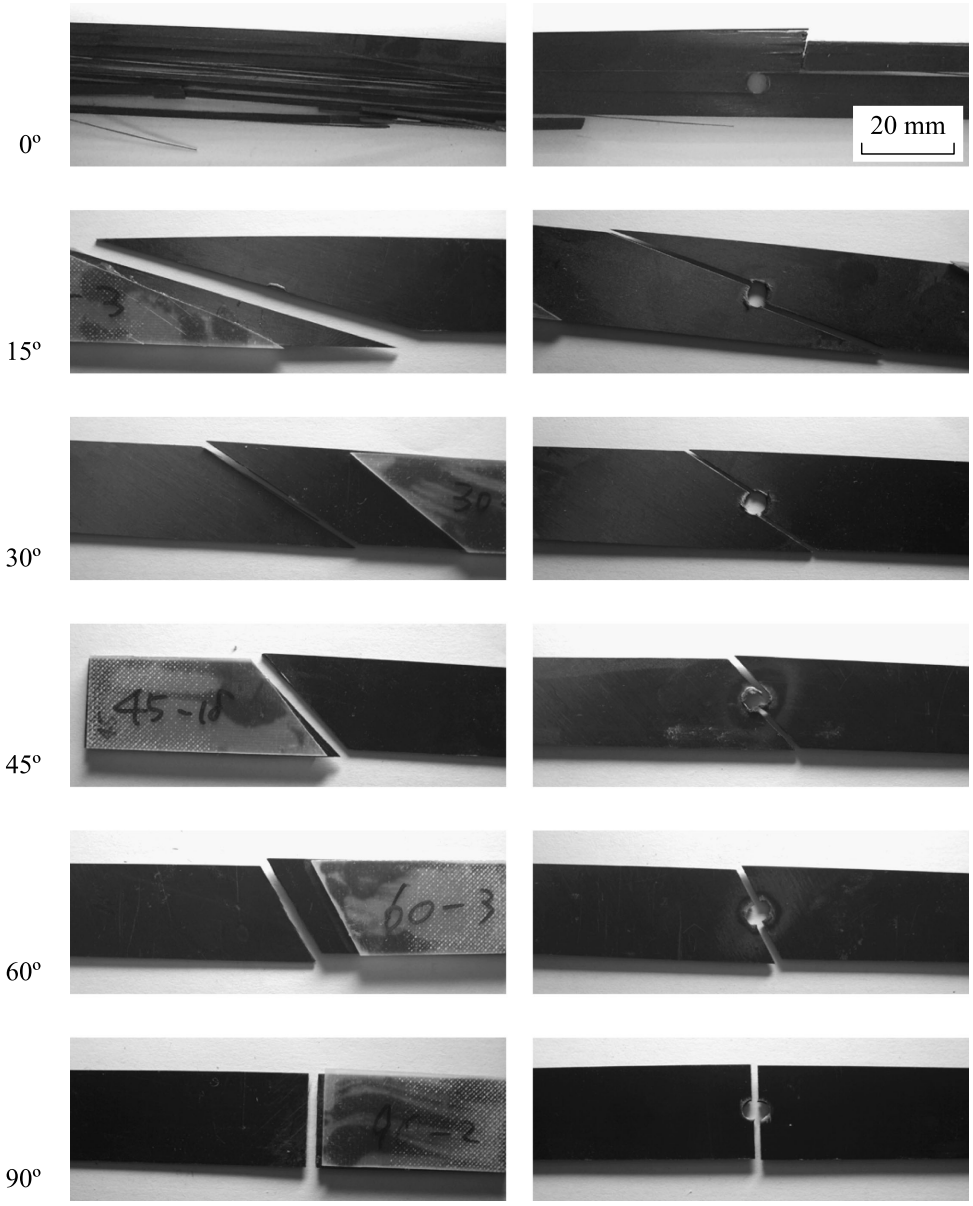

(a) Intact specimen (b) Notched specimen (D = 4 mm)

Figure 7. Typical fracture patterns of the off-axis specimens.

$\theta = 15°$ and 30° because of the shear-coupling and the nonlinearity for the shear deformation in the constitutive equation that was neglected in the analysis.

Figure 10 depicts the nominal stress that the Tsai–Hill criterion is satisfied at distance r from the hole edge for the hole diameter $D = 2$ mm, where the nominal

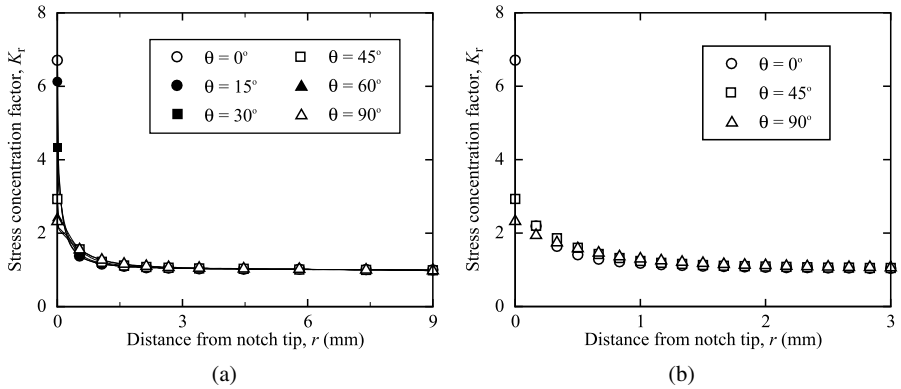

Figure 8. Distribution of the stress concentration factor for the model of $D = 2$ mm. (a) All off-axis angles. (b) Magnified view for $\theta = 0°, 45°, 90°$.

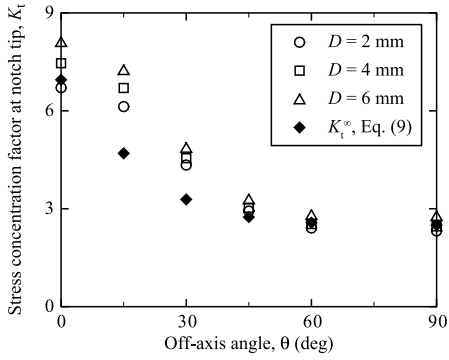

Figure 9. Calculated stress concentration factor at the hole edge.

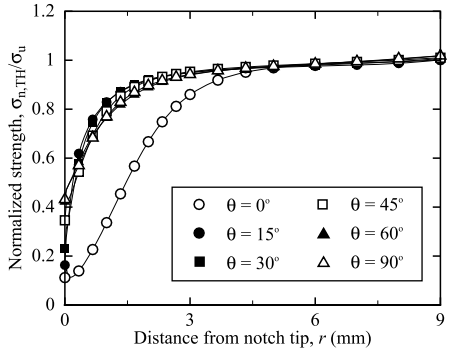

Figure 10. Distribution of the normalized strength that satisfied the Tsai–Hill criterion at the distance r from the hole edge ($D = 2$ mm).

Table 2.
Characteristic distance determined by the Tsai–Hill criterion

Off-axis angle	$D = 2$ mm	$D = 4$ mm	$D = 6$ mm	Average
0°	2.93	4.20	4.60	3.91
15°	0.53	0.50	0.77	0.60
30°	0.37	0.47	0.67	0.50
45°	0.37	0.47	0.53	0.46
60°	0.033	0	0	0.011
90°	0	0	0	0

Unit: mm.

stress is normalized by the tensile strength of the unnotched specimen. A different tendency in the normalized strength was obtained near the hole for $\theta = 0°$ due to the large orthotropic properties. Similar results on the normalized strength were obtained in the other hole diameters.

5.3. PSC

We defined the distance r where the normalized strength was equal to the measured strength ratio β depicted in Fig. 6, i.e., $\sigma_{n,TH} = \sigma_{n,C} = \beta\sigma_u$, as the characteristic distance r^*; the obtained r^* was listed in Table 2. The characteristic distance r^* was small in the off-axis and 90°-specimens. The effect of hole diameter on the characteristic distance was relatively small in all the off-axis angle; the little dependence of the characteristic distance on the notch size coincided with the previous study [1].

The ratio of the notched strength to the unnotched strength, $\beta = \sigma_{n,C}/\sigma_u$, is predicted by the following equation [2, 3],

$$\beta = \frac{2}{2 + \xi^2 + 3\xi^4 - (K_t - 3)(5\xi^6 - 7\xi^8)}, \tag{10}$$

where $\xi = \rho/(\rho + r^*)$ for the holed specimens. Figure 6 compares the strength ratio β predicted by equation (10) with the experimental results. Here, the averaged characteristic distance r^* and the theoretical stress concentration factor at the hole edge K_t^∞ were applied to equation (10). The strength predicted by the PSC agreed well with the measured strength. These results demonstrated the validity of the characteristic distance r^* determined by the Tsai–Hill criterion. The predicted strength ratio for 15° and 30° specimens was slightly larger than the experimental results. The prediction used the stress concentration factor of an infinite plate, which was smaller than that of a specimen with finite width at the off-axis angle of 15° and 30° (Fig. 9) because of the shear-coupling. Equation (10) then yielded larger strength ratio than the experimental results at these off-axis angles. This result suggested that the use of equation (9) will need careful investigation on the stress concentration at some off-axis angles with large shear-coupling.

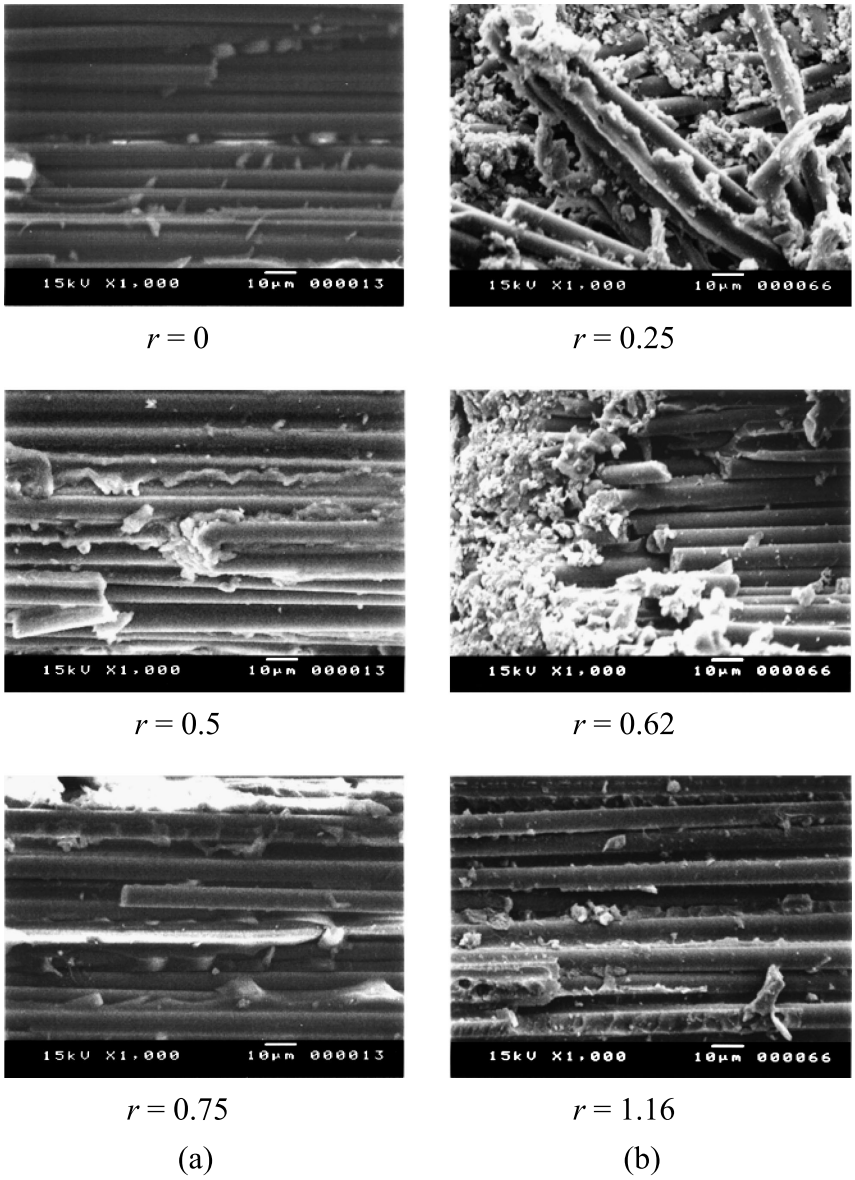

Figure 11. Fractured surfaces observed by SEM for 15° specimens. (a) $D = 2$ mm; (b) $D = 6$ mm.

Furthermore, the fractured surfaces of the holed unidirectional laminates were observed by SEM to clarify the physical meaning of the characteristic distance. Tanaka *et al.* [11] experimentally indicated that the fracture mode changed from the tensile (fiber breakage) mode to the shear (matrix) mode at the off-axis angle of $\theta = 15°$–$20°$. Figure 11 then depicts the typical fractured surfaces observed in the 15° specimens with $D = 2$ and 6 mm. The fracture line had the inclined angle

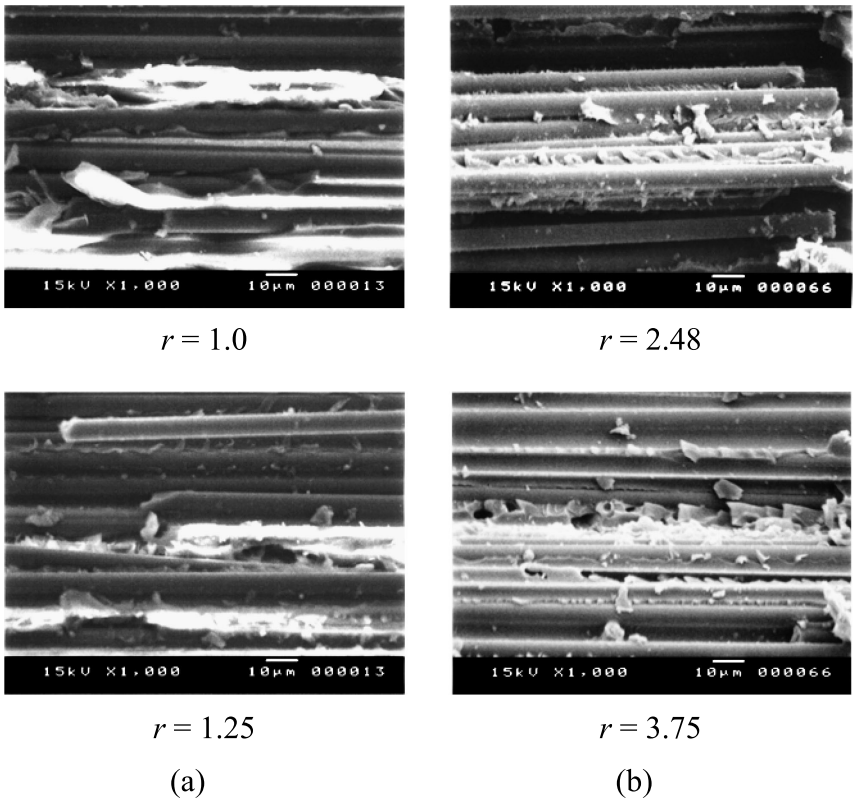

Figure 11. (Continued.)

of 15° from the longitudinal direction; we defined the coordinate r as the position projected onto the y-axis in the minimum cross-section. A few fiber breakages were observed near $r = r^*$, and many bare fibers were visible within the characteristic distance r^* in the specimen with $D = 2$ mm (Fig. 11(a)). The fibers were covered by the epoxy resin at the position away from the hole. Many fiber breakages appeared within the characteristic distance in the specimen with $D = 6$ mm (Fig. 11(b)). Similarly to Fig. 11(a), few fiber breakages could be observed and the fibers were covered by the resin outside that region. These fractured surfaces observed away from the hole were similar to the unnotched specimen with the same off-axis angle. Thus, the fracture mode could change at the characteristic distance. We observed the change in the fracture mode at the characteristic distance in the other off-axis angle of 5° and 10° in the other set of experiments. If we considered r^* as the damage region at the hole edge, these observations suggested that the microscopic damage, i.e., fiber breakage, was first generated within the area of $r \leqslant r^*$; brittle extension of the matrix crack occurred almost concurrently with the initiation of the initial damage. Figure 12 schematically illustrates the fractured modes for small and large off-axis angles. Unlike the fractured surfaces for a small off-axis angle (Figs 11

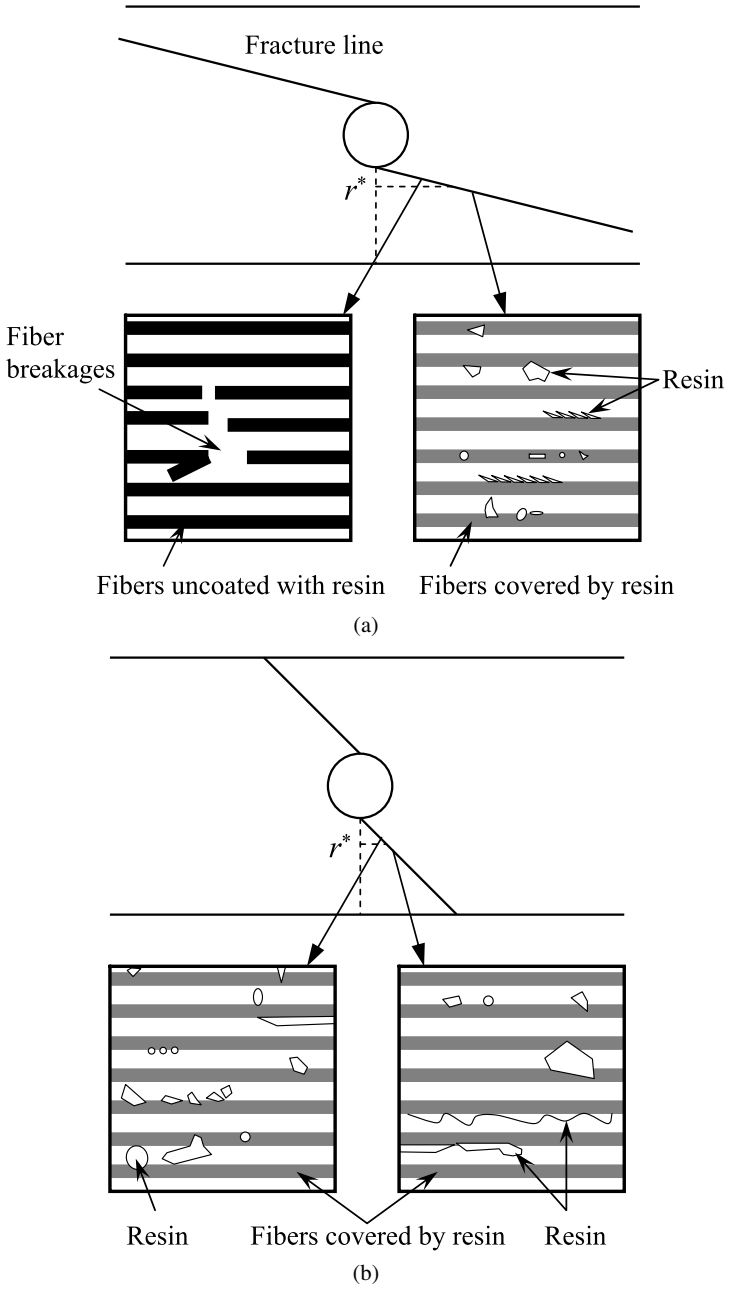

Figure 12. Schematics of fracture modes for (a) small and (b) large off-axis angles.

and 12(a)), significant change in the fractured surfaces with the position r could not be observed in the specimens with a large off-axis angle (Fig. 12(b)). Few fiber breakages appeared and the fibers were coated with the resin except the misaligned

fibers, since the initial damage was the matrix cracking in the shear mode, not the fiber breakage.

6. Conclusions

This paper describes a fracture criterion for holed CFRP unidirectional laminates with large orthotropic properties. We introduced the Tsai–Hill criterion into the process of determining the characteristic distance in the PSC. This fracture criterion was a simple approach for estimating notched strength, since only the strengths in the material's principal coordinate were needed regardless of the magnitude of the orthotropic properties and the damage mode. The notched strength that was predicted by the PSC combined with the Tsai–Hill criterion presented in this study agreed well with the measured strength. This result confirmed the characteristic distance where the nominal stress that yielded the stress field satisfying the Tsai–Hill criterion was equal to the measured notched strength. Furthermore, the observation of the fractured surfaces indicated that the characteristic distance could correspond to the region where the initial damage, such as fiber breakage, was generated.

Acknowledgements

The authors thank Mr. H. Uenishi (Ehime University) for great efforts in the experiments and observations.

References

1. J. Awerbuch and M. S. Madhukar, Notched strength of composite laminates: predictions and experiments — a review, *J. Reinf. Plast. Compos.* **4**, 3–159 (1985).
2. J. M. Whitney and R. J. Nuismer, Stress fracture criteria for laminated composites containing stress concentrations, *J. Compos. Mater.* **8**, 253–264 (1974).
3. R. J. Nuismer and J. M. Whitney, Uniaxial failure of composite laminates containing stress concentrations, *Fract. Mech. Compos., ASTM STP* **593**, 117–142 (1975).
4. R. B. Pipes, R. C. Wetherhold and J. W. Gillespie Jr., Notched strength of composite material, *J. Compos. Mater.* **13**, 148–160 (1979).
5. J. S. Huh and W. Hwang, Fatigue life prediction of circular notched CFRP laminates, *Compos. Struct.* **44**, 163–168 (1999).
6. H. M. S. Belmonte, C. I. C. Manger, S. L. Ogin, P. A. Smith and R. Lewin, Characterisation and modelling of the notched tensile fracture of woven quasi-isotropic GFRP laminates, *Compos. Sci. Technol.* **61**, 585–597 (2001).
7. H. M. S. Belmonte, S. L. Ogin, P. A. Smith and R. Lewin, A physically-based model for the notched strength of woven quasi-isotropic CFRP laminates, *Compos. Part A* **35**, 763–778 (2004).
8. R. Hill, A theory of the yielding and plastic flow of anisotropic metals, *Proc. Royal Soc. Lond. A* **193**, 281–297 (1948).
9. S. W. Tsai and E. M. Wu, A general theory of strength for anisotropic materials, *J. Compos. Mater.* **5**, 58–80 (1971).
10. H. Tanaka, K. Tanaka, Y. Akiniwa and M. Hojo, Tensile failure of unidirectional CFRP containing stress concentrations, *J. Soc. Mater. Sci. Japan* **40**, 540–546 (1991) (in Japanese).

11. H. Tanaka, K. Tanaka, T. Inoguchi and M. Hojo, Prediction for split initiation in notched unidirectional carbon/epoxy laminate under tensile loading, *Trans. Japan Soc. Mech. Eng.* **A57**, 789–795 (1991) (in Japanese).
12. K. Ogi, T. Yamamoto, S. Yashiro and T. Watanabe, Fracture criteria for unidirectional discontinuous fiber reinforced plastics with side notches, *J. Soc. Mater. Sci. Japan* **57**, 725–731 (2008) (in Japanese).
13. H. Hyakutake, H. Nishitani and T. Hagio, Fracture criterion of notched plates of FRP, *JSME Int. J. Ser. 1* **32**, 300–306 (1989).
14. H. Hyakutake, T. Hagio and H. Nishitani, Fracture of FRP plates containing a circular hole under tension, *Trans. Japan Soc. Mech. Eng.* **A55**, 112–117 (1989) (in Japanese).
15. H. Hyakutake and T. Yamamoto, Fracture criterion for tension loaded FRP plates with open holes, *J. Soc. Mater. Sci. Japan* **43**, 679–683 (1994) (in Japanese).
16. C. T. Sun and I. Chung, An oblique end-tab design for testing off-axis composite specimens, *Composites* **24**, 619–623 (1993).
17. F. Pierron and A. Vautrin, The 10° off-axis tensile test: a critical approach, *Compos. Sci. Technol.* **56**, 483–488 (1996).
18. S. G. Lekhnitskii, *Anisotropic Plates*. Gordon and Breach, New York, USA (1968).

Appendix

The plane stress condition is assumed for a unidirectional laminate, and the material principal coordinate system (1–2) is rotated by the angle θ from the global coordinate system (x–y) as depicted in Fig. 1. The stress components in the principal coordinate system are calculated using those in the global coordinate by

$$\begin{bmatrix} \sigma_1 \\ \sigma_2 \\ \sigma_6 \end{bmatrix} = \begin{bmatrix} m^2 & n^2 & 2mn \\ n^2 & m^2 & -2mn \\ -mn & mn & m^2 - n^2 \end{bmatrix} \begin{bmatrix} \sigma_x \\ \sigma_y \\ \sigma_{xy} \end{bmatrix}, \tag{11}$$

where $m = \cos\theta$ and $n = \sin\theta$; the subscripts 1, 2 and 6 represent the longitudinal, transverse and in-plane shear components.

In notched specimens, the stress components at the distance r from the notch tip are expressed by

$$\sigma_{1\mathrm{r}} = K_{1\mathrm{r}}\sigma_{\mathrm{n}}, \quad \sigma_{2\mathrm{r}} = K_{2\mathrm{r}}\sigma_{\mathrm{n}}, \quad \sigma_{6\mathrm{r}} = K_{6\mathrm{r}}\sigma_{\mathrm{n}}, \tag{12}$$

where σ_{n} is the average tensile stress in the minimum cross-sectional area, termed nominal stress in this study. $K_{i\mathrm{r}}$ ($i = 1, 2, 6$) is the ratio of the stress component at a distance r to σ_{n}. The stress component σ_x at a distance r from the notch tip, $\sigma_x = \sigma_{\mathrm{r}}$, is represented in terms of σ_{n} by using equations (11) and (12):

$$\sigma_{\mathrm{r}} = K_{\mathrm{r}}(r, \rho, \theta)\sigma_{\mathrm{n}}. \tag{13}$$

Here, $K_{\mathrm{r}}(r, \rho, \theta)$ is the arranged factor and is represented by equation (6).

The Tsai–Hill criterion for an orthotropic plate under the plane stress condition is represented by equation (1). Substituting equation (12) into equation (1) results in the nominal stress that satisfies the Tsai–Hill criterion at a distance r, $\sigma_{\mathrm{n,TH}}$, as

indicated in equation (2). We can obtain the stress component σ_x when the Tsai–Hill criterion is satisfied at a distance r, $\sigma_x = \sigma_{\mathrm{r,TH}}$, as equation (3) by substituting $\sigma_{\mathrm{n,TH}}$ into equation (13).

The ratio of the nominal stress that satisfies the Tsai–Hill criterion at a distance r to the tensile strength of the unnotched specimen is derived from equations (2) and (4), and is expressed by

$$\frac{\sigma_{\mathrm{n,TH}}(r,\rho,\theta)}{\sigma_{\mathrm{u}}(\theta)} = \sqrt{\frac{m^2(m^2-n^2)+n^4/s_2^2+m^2n^2/s_6^2}{K_{1\mathrm{r}}(K_{1\mathrm{r}}-K_{2\mathrm{r}})+K_{2\mathrm{r}}^2/s_2^2+K_{6\mathrm{r}}^2/s_6^2}}, \tag{14}$$

where $s_i = \sigma_{i\mathrm{u}}/\sigma_{1\mathrm{u}}$ $(i = 2, 6)$. This expression is used in Fig. 9.